Molecular Modeling and Simulations of AOT−Water Reverse Micelles in Isooctane: Structural and Dynamic Properties

Stéphane Abel,[†,‡] Fabio Sterpone,[†] Sanjoy Bandyopadhyay,[§] and Massimo Marchi*[,†]

Commissariat à l'Énergie Atomique, DSV-DBJC-SBFM, URA 2096/CNRS, Centre d'Études, Saclay, 91191 Gif-sur-Yvette Cedex, France, Laboratoire d'Imagerie Parametrique, UMR 7623 CNRS, Universite Pierre et Marie Curie, 15, rue de l'Ecole de Medecine, 75006 Paris Cedex, France, and Molecular Modeling Laboratory, Department of Chemistry, Indian Institute of Technology, Kharagpur - 721302, India

Received: June 30, 2004; In Final Form: September 24, 2004

This paper reports results from four nanosecond constant pressure and temperature simulations of sodium di-2-ethylhexylsulfoccinate (AOT) and water reverse micelles (RMs) in an apolar solvent, isooctane. The concentration of our simulated micelles was chosen to fall in a range which in nature corresponds to the L_2 phase of the ternary system. To our knowledge, this is the first study to develop a full molecular model for AOT micelles in an apolar solvent. We address here the problems of the shape of the RM and of its hydrophilic inner core. For the AOT−water system, we obtain nonspherical aggregates of elliptical shape with ratios between major axis, *a*, and minor axis, *c*, between 1.24 and 1.41. The hydrophilic inner core is also ellipsoidal with larger *a*/*c* ratios. Although experiments indicate that the L_2 of the AOT−water−oil system is likely to be polydisperse, we can only simulate monodisperse RMs. Nonetheless, our simulations are capable of reproducing well the dimensions of the water pool and their dependence on W_0, as determined in some small-angle neutron and X-ray scattering experiments. Stimulated by recent experiments showing anomalous behavior of the confined water for AOT−water RMs, we have also investigated the static and dynamic properties of the RM's water inner core. From smaller micelles to larger, we find that the properties of confined water tend to near those of bulk water. In particular, we find that the solvation of the counterions is more effective in larger micelles and that diffusion of water is retarded with respect to bulk more in smaller RMs than in larger.

I. Introduction

The important role that reverse micelles (RMs) play in biochemistry has been recognized since the beginning of the 1940s.[1] In the past, they have been employed to perform enzymatic reactions as bioreactors[2−4] or to solubilize biomolecules[5] that were otherwise nonsoluble.[6] The structure of reverse micelles has been studied by various physical methods: fluorescence,[7,8] NMR,[9,10] neutron scattering,[11] X-ray scattering, quasi-elastic light scattering, calorimetry,[10] and infrared[12,13] and teraHertz (THz)[14] spectroscopies. In addition, other techniques such as diffusion,[15,16] acoustics, and densitometric analysis[17] can be used to gather information on the aggregation and volumetric properties.

All these approaches have provided nonexhaustive structural information on RMs. For instance, details on the shape, the aggregation, or the properties of the hydrophilic inner core of RMs can be derived by the experiments mentioned before only indirectly, through appropriate models. In this paper, we would like to make a few steps forward in the investigation of RMs in apolar solvents, providing an atomistic description and modeling of a specific oil/detergent/water ternary system.

We are not the first in this endeavor as, in recent years, molecular dynamics simulations of RMs have began to appear. To our knowledge, the first molecular modeling with full atomistic details was carried out by Tobias and Klein[18] on a calcium carbonate−sulfonate reverse micelle. Since then simulations of $C_{12}E_2$ RMs in organic solvents[19] and of fluorosurfactant RMs in CO_2[20−23] have also appeared.

In this article, we focus on the reverse micelles formed by sodium di-2-ethylhexylsulfoccinate (AOT) and water in isooctane. This ternary system shows a complex phase diagram. Its RM, L_2, isotropic phase has been extensively studied by a variety of experimental techniques. In particular, light, neutron, and X-ray scattering results for L_2 at low water concentrations all are consistent with the picture of a droplet of water, the inner core of the aggregate, surrounded by the detergent in contact with the oil.[24−26] Small-angle neutron[26−28] and X-ray scattering,[17,29] SANS and SAXS, respectively, have provided indirect information on the shape and dimensions of the RMs of AOT in various organic solvents. Given the low sensitivity of these techniques, results on the shape and the dimensions, radius of gyration, are sometimes contradictory, especially for the smallest micelles.

Other experiments have pointed out the peculiar nature of the water in the inner core.[30] Indeed, volumetric and dielectric properties of water in RMs and in the bulk are strikingly different. According to ref 17, compressibilities and changes in the volume of water depend strongly on the size of the micelle due to increasing amounts of "free water". Also, experiments based on far-infrared[13] and teraHertz time-domain spectroscopies[12,31] have shown significant changes in the absorption peaks with the size of the RM's hydrophilic core. Although the

* To whom correspondence should be addressed. E-mail: mmarchi@cea.fr.
† Commissariat à l'Énergie Atomique, DSV-DBJC-SBFM, Centre d'Études.
‡ Laboratoire d'Imagerie Parametrique, UMR 7623 CNRS, Universite Pierre et Marie Curie.
§ Molecular Modeling Laboratory, Department of Chemistry, Indian Institute of Technology.

10.1021/jp047138e CCC: $27.50
Published on Web 11/20/2004

existence of water molecules strongly bound to the surfactant headgroup has been invoked to explain these findings, a full understanding of these anomalous properties of water in confinement is still lacking.

So far, no atomistic modeling of the water−AOT−oil ternary system has been reported. In the past, only simplified models have been proposed and investigated. In particular, only the inner core of the micelle (water and the AOT counterions) was atomistically modeled, whereas the organic solvent and the detergent were represented as a continuum in a mean field spirit.[32−35] Unfortunately, these continuum methods can provide no information regarding the structure of the detergent and its interaction with either oil or water. In addition, in all of these investigations a spherical shape of the RM inner core is assumed, thus neglecting water penetration in the hydrophobic region and the deformations of the micelle itself.

In this paper, we report results from extensive molecular dynamics (MD) simulations of a few reverse micelles of AOT and water in isooctane. We have studied four micelles distinct by their sizes or by the way their initial conditions were chosen. We simulated three RMs with different water-to-surfactant molar ratios, $W_0 = [H_2O]/[AOT] = 3$, 5, and 7, and with sufficient solvent to mimic the concentration conditions of the L_2 phase of the corresponding ternary system. An additional and independent simulation for $W_0 = 3$ in the same conditions of solvent concentration was also run. Each of the simulation runs lasted 3.5 ns, including equilibration, for a total of 14 ns. In the next section, we discuss the methodological issues related to our modeling work, the preparation procedure of the systems, and the force field used in the MD simulations. This will be followed by the results obtained from our simulations and by their interpretation.

II. Methods

A. System and Force Fields. This study is focused on the static and dynamic properties of three reverse micelles with a water-to-surfactant molar ratio, $W_0 = [H_2O]/[AOT]$, of 3, 5, and 7. Four inverted micelles were studied: two of $W_0 = 3$, named RM43^a and RM43^b, each containing 43 molecules of AOT but prepared with different procedures; one each for $W_0 = 5$, RM64, and $W_0 = 7$, RM82, containing 64 and 82 AOT molecules, respectively. The number of surfactant molecules for a given W_0 was taken from estimates reported in ref 17 and based on SAXS experiments. To reduce the system size of RM82, the largest micelle, the number of surfactant molecules and water molecules was reduced by 10% with respect to the SAXS estimate. In addition to the water in the interior, sodium ions were also added to neutralize the systems. The micelles were solvated in a box of isooctane molecules. The number of solvent molecules and the dimensions of the simulation box were chosen to be compatible with the RM phase, L_2, of the AOT/water/isooctane mixture,[36] corresponding to an isooctane molar fraction of at least 80%.

An all atom potential model was adopted for AOT, water, and isooctane. The force field and topology for the AOT molecule were derived from the CHARMM27 all atom parameters for lipids[37] and adapted recently for an AOT/water system,[38] whereas water was described by the well-known TIP3P model.[39] This choice of water model is consistent with the CHARMM force field for lipids. The isooctane force field was again obtained from the CHARMM model of *n*-pentane by replacing the three hydrogens of a terminal methyl group with three methyls. The additional bonded intramolecular interactions of this molecule were modeled from the geometry of isooctane in the gas phase. Simulations of liquid isooctane at atmospheric pressure and $T = 300$ K showed that our set of parameters is able to reproduce well the crucial properties of the liquid, such as density, compressibility, and diffusion (data not shown). Full details of our force field are given in the Supporting Information.

TABLE 1: List of the Parameters Used to Set Up the Initial Conformations of the Reverse Micelle Systems[a]

micelle	W_0	R	n_{AOT}	n_{H_20}	n_{Iso}	a_{to}	t (ns)
RM43^a	3	8	43	129	1048	60.6	3.0
RM43^b	3	8	43	129	1047	64.5	3.0
RM64	5	11	64	320	1337	67.55	3.0
RM82	7	14	82	574	1251	69.3	3.0

[a] R is the radius in Å of the initial water−sodium sphere for each micelle. n_{AOT}, n_{H_2O}, and n_{Iso} are the number of AOT, H_2O, and isooctane molecules composing the simulated systems. a_{to} is the initial cell parameter of the truncated octahedron simulation cell. t is the simulation time for each system, not including equilibration. n_{AOT} and R were taken directly from ref 17.

In AOT, three asymmetric carbons produce eight distinct stereoisomers. It is not known which of these isomers is dominant in industrially available AOT. In this study, only one of these, the planar R(C1)R(C5)S(C14) stereoisomer (see the Supporting Information for the meaning of the atom labels) was selected to build the models of reverse micelles. Because of the high flexibility of AOT, other stereoisomers, or mixtures of them, are unlikely to affect significantly the structural properties of disordered aggregates, such as micelles.

B. Simulation Procedures. The preparation of the starting conformations of the three micelle sizes was the initial step of all our simulations. We first constructed the hydrophilic inner part of the micelle, creating spherical water clusters by enclosing n_{H_2O} water molecules in a sphere of radius R. The parameters R and n_{H_2O} used for each micellar system are reported in Table 1.

For systems RM43^a, RM64, and RM82, the hydrophilic core was prepared by selecting a spherical water cluster of an appropriate radius R from the final configurations of three 40 ps MD runs of 1024 bulk water molecules simulated in a cubic box at $T = 300$ K. The water density of these three bulk runs and the radii R of the spherical core were chosen according to parameters estimated in ref 17. The counterions were generated by randomly replacing water molecules of the cluster with Na^+.

In alternative, the water cluster RM43^b was prepared by performing a series of molecular dynamic simulations of 129 water molecules and 43 Na^+ constrained to a sphere of decreasing radius R'. Such a constraint was imposed by using an external radial potential on each atom of the type

$$V_{ext} = \frac{A}{|r - R'|^{12}} \quad (1)$$

where r, the distance between the center of mass and each atom, is always $\leq R'$. A is a parameter whose value was arbitrarily chosen as the C_{12} Lennard-Jones parameters of TIP3P water. The value of R' was first set at 20 Å and gradually reduced by 4 Å each time in four simulation steps to $R' = 8$ Å. Each simulation was carried out at $T = 500$, to speed up equilibration, and lasted 40 ps.

To build up the AOT micelle around the water−ion clusters, we used again two distinct techniques (see Table 1 for a summary of the RM's initial parameters). For systems RM43^a, RM64, and RM82, the corresponding AOT molecules in an extended conformation were placed by hand on a sphere, tail

pointing toward the exterior, around the preprepared water−ion clusters using the visualization program DS ViewerPro by Accelrys.

For system RM43^b, we followed an alternative strategy. First, by simple translation of 20 Å in the three directions we generated 64 replicas of an AOT molecule in an extended conformation in a three-dimensional cubic grid. Of these, we eliminated 21 molecules at random to obtain the required number of AOT molecules. Second, we introduced a Lennard-Jones ion of $\sigma = 12$ Å and $\epsilon = 4$ kcal mol^{-1} and charge of $+43e$ at 20 Å from the closest AOT replicas. Third, we ran a MD simulation of this system at 500 K and no spherical cutoff, all interactions included, for 400 ps. After this MD trajectory, we found that all AOT molecules had their charged headgroup at about 10 Å from the Lennard-Jones atom with their tails oriented on the outside. Finally, we replaced the Lennard-Jones ion with the previously generated water−ion cluster.

Following the preparation phase, these four systems were equilibrated at 500 K with a spherical cutoff of 10 Å for 500 ps, during which the water and the AOT headgroups were blocked. Subsequently, each system was inserted in a periodically replicated primitive body-centered cubic (bcc) box filled with isooctane. Such a simulation box corresponds to a truncated octahedron box of side length $a\sqrt{3}/2$, where a is the primitive bcc axis.

To simulate the RMs in conditions similar to a L_2 phase,[36] the size of the simulation cell was chosen to ensure a concentration of AOT/water in isooctane of less than 30 by weight. In Table 1, we supply the initial cell parameters of the truncated octahedron simulation box and the number of isooctane molecules added to each RM.

The equilibration of the solvated RMs proceeded in two steps. First, the solvent was relaxed for 200 ps at 500 K with the RM complex frozen. Second, the system was suddenly frozen at 0 K and then monotonically heated to 300 K in 300 ps. Specifically, each 0.012 ps the atomic velocities were rescaled to attain a temperature $T = T + \Delta T$, where ΔT was chosen so that $T = 300$ K after 300 ps. After equilibration, the four systems were simulated in the *NPT* ensemble ($P = 0.1$ MPa, $T = 300$ K) for 3 ns after an additional equilibration of 50 ps.

To compare the effect of the reverse micelles with the bulk solvent and water, two additional simulations were performed in the *NPT* ensemble at the same thermodynamic conditions ($P = 0.1$ MPa and $T = 300$ K). These systems contained 216 molecules of isooctane and 512 molecules of TIP3 water in two cubic boxes and were simulated for 1 ns.

C. Molecular Dynamics. To simulate the *NPT* ensemble, we have used a method based on the extended system approach.[40−43] This technique involves adding extra (virtual) dynamical variables to the system coordinates and momenta to control temperature and pressure.

Throughout this study, we have used the atom group scaling algorithm of ref 44 to integrate the equations of motion of our systems. This algorithm is a five time step r-RESPA (reversible reference system propagation algorithm)[45] integration scheme with a Liouvillean separation in three nonbonded shells, with smooth particle mesh Ewald (SPME)[46] to handle electrostatic interactions, and constraints on covalent bonds entailing hydrogen atoms. The SPME parameters were chosen so as to maintain a relative error on the electrostatic interaction below 0.1%. To this purpose, we used a converge parameter $\alpha = 0.43$ Å^{-1}. For all systems, a fifth-order B-spline took care of the SPME charge interpolation. An 80-point grid in each Cartesian direction was used for all micelles except for RM43^a where a 64-point grid was adopted instead.

TABLE 2: Cell Parameters Averaged over the Whole Length of the Trajectories[a]

micelle	RM43^a	RM43^b	RM64	RM82
$\langle a_{to} \rangle$	64.73	64.75	70.82	70.60
$\langle V_{Cell} \rangle$	321340.7	321713.5	421036.4	416894.9
$\sigma_{V_{Cell}}$	38	38	41	41
[C]	1.25	1.23	1.54	2.90
ρ	0.728	0.728	0.737	0.755

[a] The symbol $\langle ... \rangle$ stands for ensemble average. $\langle a_{to} \rangle$ is the average cell parameter of the truncated octahedron simulation cell. $\langle V_{Cell} \rangle$ and $\langle \sigma_{V_{Cell}} \rangle$ are the average total cell volume and its statistical deviation. [C] is the micellar concentration in mM. ρ is the averaged density of the system in g/cm^3. The statistical error on the density is less than 0.1%.

Finally, for each trajectory run in the *NPT* ensemble, we saved the system atomic coordinates once every 240 fs. The parallel and sequential versions of the program ORAC[47] were used throughout this work to perform simulation and analysis of the trajectories.

III. Results

A. Size and Shape of the Reverse Micelles. As shown in Table 2, the concentration of the micelles studied here is between 1.25 mM for RM43 and 2.90 mM for RM82, i.e., from 1.3 to 3 times the critical micellar concentration (cmc) for AOT reverse micelles in isooctane, cmc = 1 mM.[36] The solvent volume fraction for RM43^a, RM43^b, and RM64 is close to 90%, whereas for RM82 this is about 82%. In the same table, we also show the computed density of the four micelles after the *NPT* run.

We first focus on the shape of the simulated micelles. SAXS and SANS experiments cannot discriminate between spherical and nonspherical shapes of aggregates in solution. Indeed, the time scale of this type of measurement is orders of magnitude larger than the characteristic rotation time of a molecular assembly such as ours, a few tens of nanoseconds at most. In addition, a certain degree of polydispersity, ≃20%, is to be expected for the L_2 phase of the AOT/water/oil system.[17,25,27,48,49]

Previous molecular dynamic simulations of realistic systems of solvated inverted micelles have found nonspherical shapes for different micelles; see for instance ref 50. In our case, all the AOT reverse micelles deformed within a few hundred picoseconds of simulation from an initial spherical object to a more complex shape. Figure 1 provides a pictorial view of the deformation of the RM64 micelle as a function of simulation time. This is a typical behavior of all our simulated RMs.

Although our micelles are highly complex geometrical objects, their shape can still be conveniently approximated by an ellipsoid. Thus, for each point of the MD trajectories we can readily compute the three semiaxes, a, b, and c, of an ellipsoid of identical mass and moment of inertia as the reverse micelle. If $I_1 > I_2 > I_3$ are the inertia principal axes of the micelle and M is its total mass, we obtain the corresponding a, b, and c from

$$I_1 = \frac{1}{5}M(a^2 + b^2)$$

$$I_2 = \frac{1}{5}M(a^2 + c^2)$$

$$I_3 = \frac{1}{5}M(b^2 + c^2) \qquad (2)$$

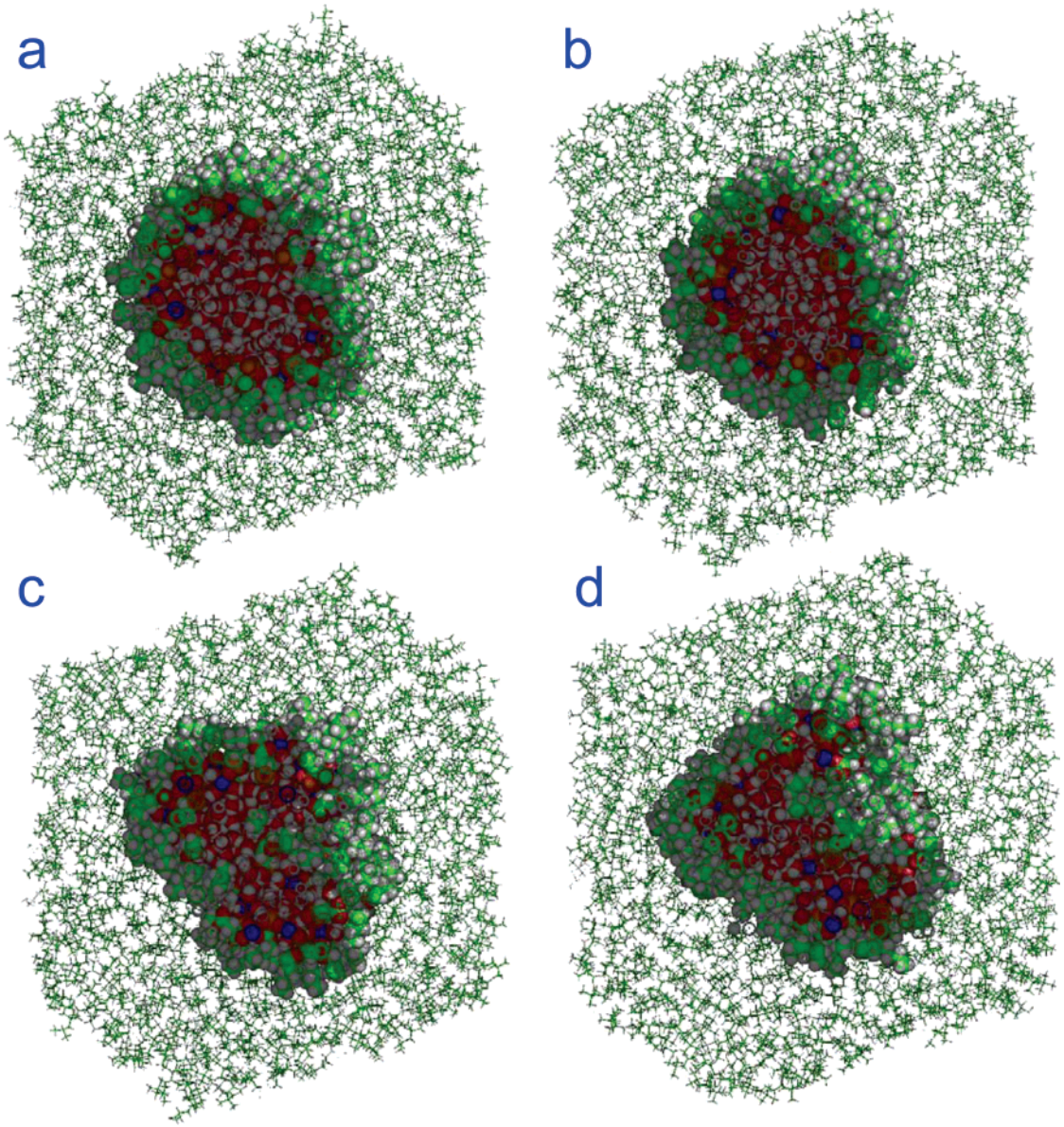

Figure 1. A pictorial view of the time evolution of the inverse micelle RM64. We present a view of the simulation box clipped by a plane orthogonal to the *X*-axis and crossing the center of mass of the AOT−water micelle. Panel a: RM64 at the end of the initial heating from 0 to 300 K (see section II.B). Panels b−d: RM64 at $t = 0.250$, 1.5, and 3.0 ns, respectively. The atoms of AOT, water, and sodium are represented by spheres, whereas the isooctane covalent bonds are shown as lines. In the picture, carbon atoms are green, hydrogen atoms gray, oxygen atoms red, and sodium atoms magenta.

We can further obtain the eccentricity of the ellipsoid, *e*, as

$$e = \sqrt{1 - \frac{c^2}{a^2}} \tag{3}$$

For a perfect sphere *e* is zero, whereas $e \rightarrow 1$ for a flat or needlelike shape.

Typically, the shape parameters, ellipsoidal semiaxes and *e*, of the simulated reverse micelles settled down to stable values after a few hundred picoseconds. In Figure 2, we show such a typical behavior for the instantaneous eccentricity of the RM43 micelle.

In Table 3, the shape parameters for all the simulated micelles are reported. Remarkably, all systems studied here show a large deviation from a spherical shape, their eccentricity being between 0.59 (RM43^a) and 0.71 (RM43^b). We notice that *e* does not increase or decrease systematically going from smaller to larger micelles, whereas for the same type of micelle, RM43, it can vary by up to 0.1 units. This deviation shows the degree of dependence on initial conditions for runs of 3 ns such as ours.

For all our RMs, the geometrical shape fluctuates around an "oblatelike" ellipsoid, $\langle b \rangle \simeq \langle c \rangle$, within the 3 ns simulations. The average of the ratio between the major and the minor semiaxes, $\langle a/c \rangle$, calculated from each micelle gives a range within 1.24 (RM43^a) and 1.41 (RM82) units. The values for a/c found here are consistent with a simulation of solvated reverse micelles by Senapati et al.[50] which found $a/c = 1.3$ for their fluoro-surfactant-based reverse micelles in carbon dioxide. For a different reverse micelle system, $C_{12}E_2$ in dodecane, Klein and co-workers[19] found instead an almost spherical shape. As for simulated regular micelles, a range of 1.01−2.3 has been found for sodium octanoate micelles[51,52] and sodium dodecyl sulfate micelles.[53]

As discussed in section II.B, for each micelle of a given W_0, the number of AOT molecules was chosen according to the experimental estimates of ref 17. To further test our molecular

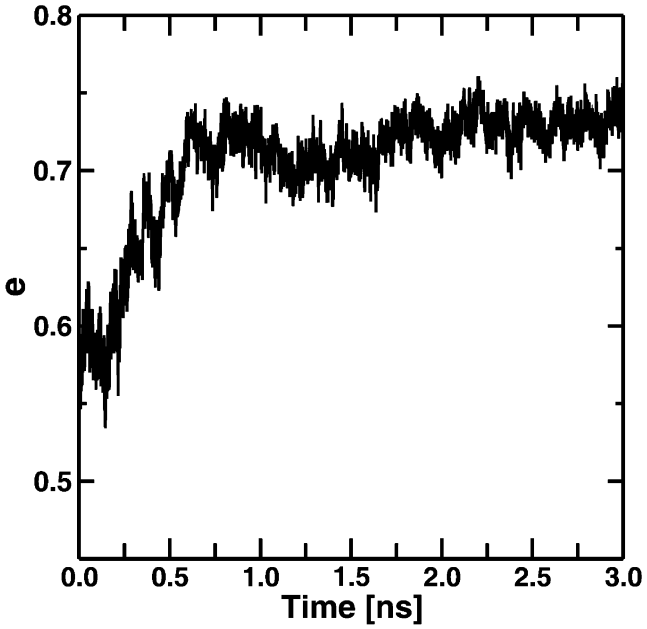

Figure 2. The evolution of eccentricity, *e*, for micelle RM43[a] for the 3 ns of our simulation.

TABLE 3: Semiaxes of the Micellar Ellipsoid[a]

simulation	*a*	*b*	*c*	$\langle a/c \rangle$	*e*
RM43[a]	21.64	18.82	17.43	1.24	0.59
core	16.52	11.94	9.77	1.69	0.81
RM43[b]	21.59	19.48	15.25	1.41	0.71
core	16.12	13.87	7.78	2.07	0.87
RM64	25.85	23.70	18.67	1.40	0.70
core	19.47	17.35	11.50	1.69	0.80
RM82	29.73	25.57	21.06	1.41	0.69
	23.22	18.22	13.86	1.67	0.80

[a] The semiaxes $a > b > c$ have been computed from the three moments of inertia according to eqs 2 and averaged over the all trajectories after discarding the initial 240 ps. The eccentricity, *e*, is obtained from eq 3. Each row of the table labeled with the simulation logo refers to the semiaxes of the entire micelle. The *core* labeled rows report the semiaxes computed for the water core. The statistical error on the semiaxes is never greater than 4%.

models, we have also carried out two additional simulations for $W_0 = 5.7$ and $W_0 = 6.5$ by eliminating 10 and 20% of AOT molecules from the system with $W_0 = 5$, respectively. The two systems were prepared following a procedure described in section II.B for RMs RM43[a], RM64, and RM82 and run for 1 ns each. The value of the ratio $\langle a/c \rangle$ obtained from these two additional simulations did not change, being around 1.4 as for the longer runs.

We have also computed the radius of gyration, or R_g, for the micelle and the water core. R_g is defined as

$$R_g^2 = \sum_i m_i (r_i - r_{cm})^2 \Big/ \sum_i m_i \qquad (4)$$

where m_i is the mass of atom *i* at distance r_i from the center of mass r_{cm} of the reverse micelle. For ellipsoidal solids of uniform density, R_g is directly obtainable from the knowledge of the three semiaxes according to the formula

$$R_g^2 = \frac{a^2 + b^2 + c^2}{5} \qquad (5)$$

Table 4 shows the computed value of R_g for the whole AOT−water aggregate, R_g^{AOT}, and its water core, R_g^w, of each investigated reverse micelle using eq 5. The R_g values computed from eq 5 agree very well, within a few percent, with results of the full calculation of eq 4.

TABLE 4: Averaged Radius, $\bar{R}$, and Radius of Gyration, R_g, of the AOT Micelles and Their Water Cores[a]

simulation	R_g^{AOT}	$\bar{R}^{AOT}$	R_g^w	$\bar{R}^w$	R_g^{hg}	R_g^{exp}	d_{Tail}	$d_{e\text{-to-e}}$
RM43[a]	15.0	19.2	10.1	12.4	11.2	12.4	6.8	9.6
RM43[b]	14.7	18.6	10.1	12.0	10.7	12.4	6.6	10.1
RM64	17.8	22.5	12.7	15.7	14.1	14.6	6.8	9.9
RM82	19.9	25.2	14.6	18.0	16.0	16.8	7.2	9.6

[a] The quantities labeled by superscripts AOT and w were computed by including all atoms of the micelle and those of the water core, respectively. The radii of gyration were obtained from the ellipsoid semiaxes reported in Table 3 by using eq 5. The average radius, $\bar{R}$, corresponds to the radius of a sphere with identical volume of the ellipsoids of Table 3. In column 6 are reported the radii of gyration obtained including in the calculation the water molecules and the non-carbon, non-hydrogen atoms of the detergent. These are directly comparable with the data in column 7 obtained by linear interpolation of the SAXS experimental values (ref 29) to our values of W_0. In the last two columns, the thickness of the hydrophobic region obtained from the average micelle radii, $d_{Tail} = \bar{R}^{AOT} - \bar{R}^w$, and the average end-to-end distance of an AOT molecule, $d_{e\text{-to-}e}$, are reported, respectively. The latter quantity has been obtained from the first peak of the end-to-end probability distribution function of Figure 4.

The values of R_g^w in Table 4 were obtained by including only contributions from the water molecules in eq 4. In the same table, R_g^{hg} values were computed including contributions from all non-carbon atoms. They compare very well with those estimated in ref 29 and labeled R_g^{exp} in the table.

We have also computed the average radius of the RMs and of its water pool, $\bar{R}$. Since both in our simulations are of ellipsoidal shape, $\bar{R}$ corresponds to the radius of the sphere having the same volume as the corresponding inner core ellipsoid, i.e., $\bar{R} = (abc)^{1/3}$. In Table 4, we report the values of $\bar{R}^{AOT}$ and $\bar{R}^w$ obtained from the ellipsoidal semiaxes of the RM and its water pool presented in Table 3, respectively.

As shown by most investigators and, in particular, in at least two SANS investigations,[27,28] the radius of the water pool, our $\bar{R}^w$, is linear in the molar ratio, W_0. Figure 3, which plots the $\bar{R}^w$ as a function of W_0 from Table 4, shows that the same linear behavior is reproduced by our simulations. In earlier works by Kotlarchyk et al.,[25,27] $\bar{R}^w$ is related to the molar ratio by the equation

$$\bar{R}^w = \frac{3v_{H_2O}}{a_0} W_0 + \frac{3V_H}{a_0} \qquad (6)$$

Here v_{H_2O} is the volume occupied by a water molecule, a_0 is the area of the AOT surface shared with water, and V_H is the volume of the water-penetrated portion of a single AOT headgroup. Based on SANS experiments on micelles with $W_0 > 8$, at 301.6 K, $3v_{H_2O}/a_0 = 1.41$ Å and $3V_H/a_0 = 12$ Å in refs 25 and 27. In a more recent work,[28] the slope and the intercept of $\bar{R}^w$ versus W_0 were estimated at 1.9 and 7 Å, respectively. The linear interpolation of our results in Figure 3 provides values for slope and intercept somewhat between those of the SANS experiments, and we find 1.4 and 8.35 Å, respectively.

We notice that the computed difference $\bar{R}^{AOT} - \bar{R}^w$ is always around 7 Å for our four micelles, whereas the length of the hydrophobic chain in its extended conformation can be estimated at around 12 Å. Two contributions concur to reduce the hydrophobic shell of the reverse micelle: (a) penetration of water in the hydrophobic region of AOT; (b) partial folding of the hydrophobic chains. The former effect is discussed in the

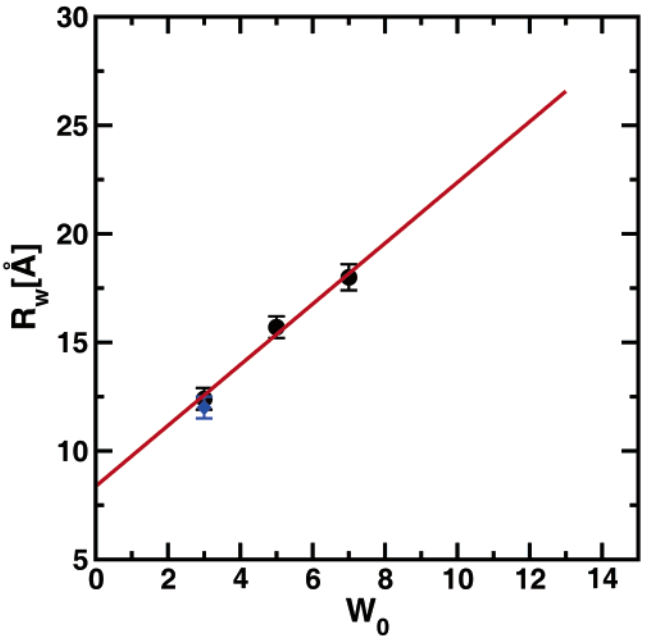

Figure 3. Plot of the radius of the water pool, $\bar{R}^w$, as a function of the molar ratio, W_0. Black circles mark the values of $\bar{R}^w$ obtained for systems RM43^a, RM64, and RM82, whereas the blue diamond refers to RM43^b. The red straight line is the linear interpolation of the four values of $\bar{R}^w$.

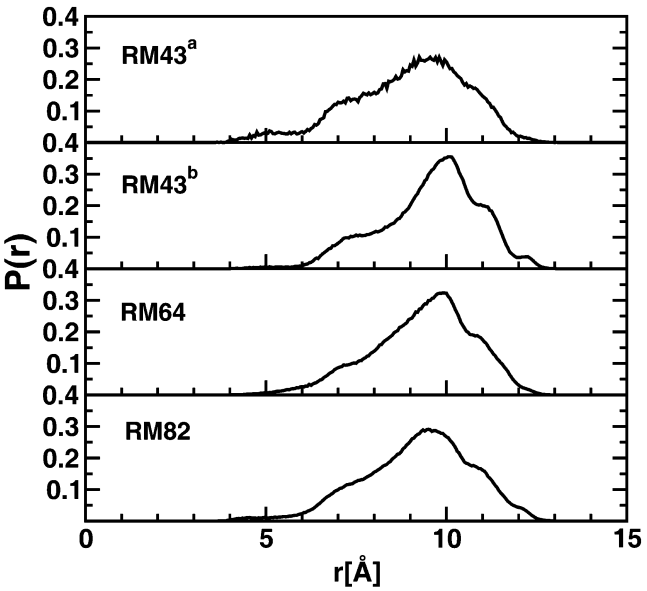

Figure 4. End-to-end distance probability distribution for the four simulated reverse micelles. $P(r)$ is the probability distribution of the distance between the sulfur and the last carbon atoms of the two hydrophobic chains. $P(r)$ is normalized to 1.

next section. As for the latter, we show in Figure 4 the probability distribution of the end-to-end distance averaged over all the AOT molecules and the length of the trajectories. Here, end-to-end distance is defined as the distance between the sulfur atom and the last carbon atoms of the two hydrophobic chains. It is clear from the picture that the AOT molecules are only partially folded, as the main maximum is found in the four cases always near 10 Å, whereas shoulders of smaller intensity exist at a lower distance of around 7 Å.

B. Density Profiles. To investigate the size and the spatial extent of the molecular components of each reverse micelle, radially averaged density profiles, or $\rho(r)$, can be straightforwardly computed from the corresponding molecular dynamic

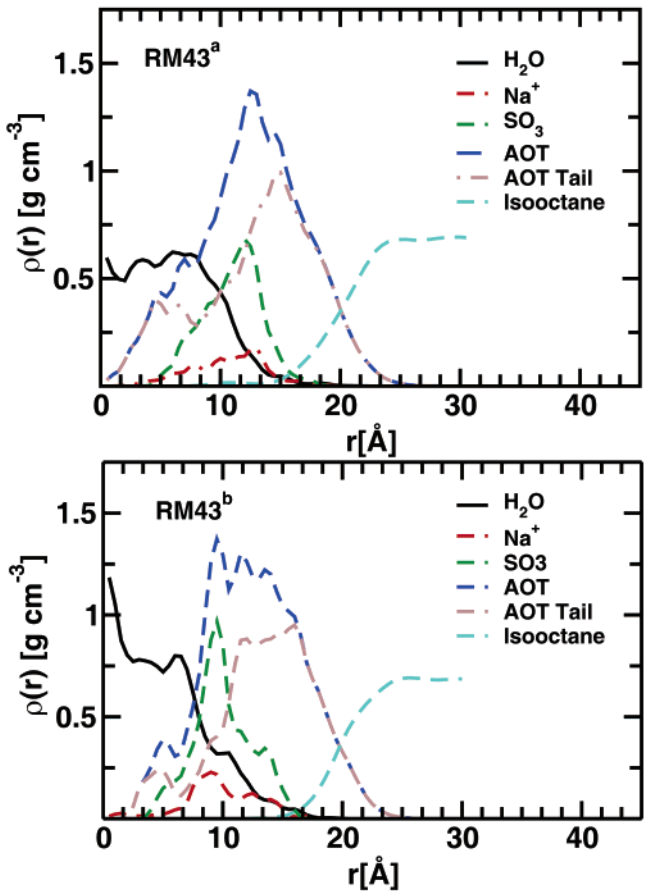

Figure 5. RM43^a, top, and RM43^b, bottom, density profiles with respect to the center of mass of the aggregates. See the text for an explanation of the legends.

trajectories. For the component a, the function $\rho_a(r)$ is defined such that

$$\rho_a(r)\,dr = \left\langle \sum_i \delta(r - r_i) \frac{m_i}{4\pi r^2} \right\rangle \tag{7}$$

where the sum $\sum_i$ extends to all the atoms of the component a, m_i is the mass of the ith atom, and $\langle ... \rangle$ is the ensemble average.

The density profiles were computed with respect to the center of mass ($r = 0$) of the aggregate. A bin width of 0.3 Å was used, and the $\rho_a(r)$ values were averaged over 3 ns of simulation for each system. We warn the reader that the nonspherical nature of our micelles will affect the interpretation of $\rho(r)$ to some extent by causing broadening and overlap of these density functions.

The calculated density profiles are shown in Figures 5 and 6. They include $\rho(r)$ values for water, the Na^+ ions, isooctane, AOT as a whole, the AOT tail, and the SO_3 group.

We first notice that the oil never penetrates in the interior of the micelles and the overlap between $\rho_{oil}(r)$ and $\rho_{H_2O}(r)$ is very small. On the contrary, the hydrophobic tails of AOT are found in some contact with the hydrophilic core. This is more marked in the smaller micelles, RM43^a and RM43^b. Indeed, Figure 5 shows that the density profiles of AOT as a whole and the profiles of its tails are identical from 0 to 6 Å for RM43^a and from 0 to 4 Å for RM43^b, blue and brown curves in the picture, respectively. Further investigations showed that in both cases one AOT molecule had one of its hydrophobic chains inside the hydrophilic core for the whole length of the runs.

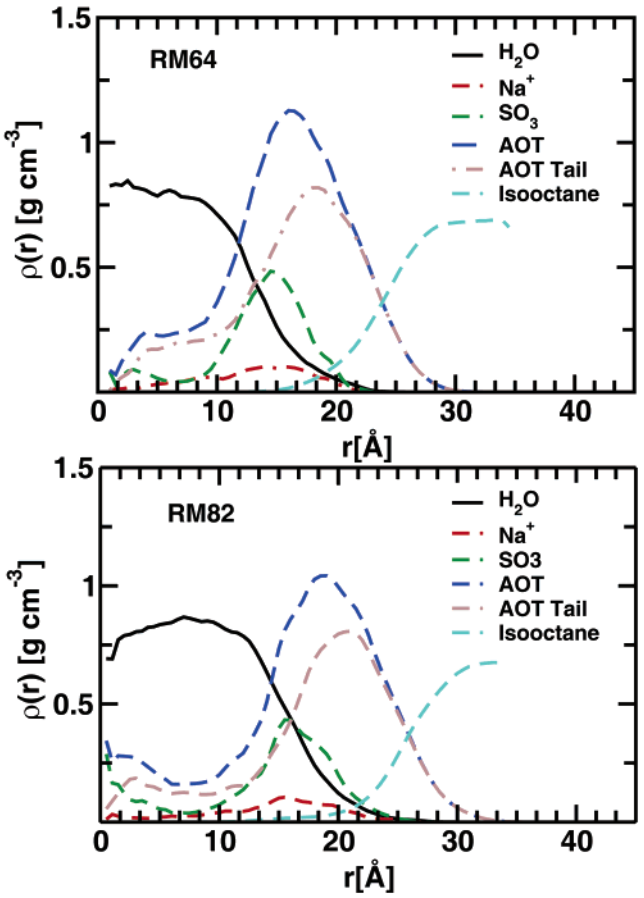

Figure 6. RM64, top, and RM82, bottom, density profiles with respect to the center of mass of the aggregate. See the text for an explanation of the legends.

The density profiles of water in the interior of the reverse micelles are nonzero in a very broad hydrophilic core region and crosses with $\rho_{AOT}(r)$ at distances increasing with the dimension of the reverse micelle. In all cases studied here, the water region contains the system ions.

Whereas for all simulations the density of the oil reaches its bulk value, the water in the micelle core is found at densities of 20% less than the bulk value or smaller.[58] This does not mean that the actual volume occupied by each water molecule is larger than that in the bulk. Decreases in density are mainly due to the penetration, discussed previously, of the hydrophobic chains of AOT inside the micelle core.

Finally, differences between the density profiles obtained from the RM43^a and RM43^b trajectories underline that the conformations of RM43 sampled by the two independent simulations are different in the details, although we find that the average potential energies of the two systems are within statistical error from each other (results not shown).

C. Hydration. To gain insights into the structural characteristics of the aqueous core, we have computed the radial pair density function, $\rho_2(r)$, of the water oxygen with sulfur and sodium. We have also obtained $\rho_2(r)$ for the couple sulfur and sodium. In Table 5, we report the corresponding number of nearest neighbors (coordination number) computed by integrating each $\rho(r)$ until the first minimum following the first peak. It is interesting to notice that the number of solvation water molecules around S increases by an average of 1 unit going from smaller to larger micelles. The same is true also for the hydration shell of Na^+ which goes from 2.1 to 3.2 neighbors for RM43^a to RM82, respectively. These findings indicate that the water core in larger micelles more efficiently hydrates the counterions and the polar heads of AOT. This is also confirmed by the decrease in the number of neighboring Na^+ atoms around the S of AOT, going from 2.4 for RM43^b to 1.7 for RM82; see the last row in Table 5.

TABLE 5: Number of Nearest Neighbors for Selected Atoms of AOT and Its Counterions[a]

interactions	RM43[a]	RM43[b]	RM64	RM82
S−H_2O[a]	5.3	6.3	7.8	8.7
Na−H_2O[b]	2.1	2.3	2.8	3.2
S−Na[c]	2.1	2.4	1.9	1.7

[a] The numbers have been obtained by integrating the pair correlation functions up to the minimum, at distance d, after the first peak. d = 5.3, 3.5, and 5.0 Å for the S−H_2O, Na−H_2O, and S−Na interactions, respectively.

TABLE 6: Surface Properties of the Four Reverse Micelles[a]

systems	SRM_v	SRM_e	ASA_{AOT}	ASA_w	a_0^v	a_0^e
RM43[a]	8751	4459	0.35	<0.01	52.0	63.1
RM43[b]	8162	4799	0.33	<0.01	51.6	66.5
RM64	10782	6861	0.33	<0.01	56.7	63.9
RM82	14502	8924	0.31	<0.01	69.5	67.3

[a] Here SRM_v and SRM_e are the surface of the micelle obtained from the Voronoi polyhedra and assuming an ellipsoid-like geometry for the micelle, respectively. See the text for an explanation. The accessible surface to the solvent of AOT and water is labeled ASA_{AOT} and ASA_w, respectively. In the final two columns, the average surface areas per AOT molecule in contact with water are reported. a_0^v was derived from the Voronoi construction, whereas a_0^e is computed assuming an ellipsoid-like geometry for the water core, see the text for further explanations. The statistical error (maximum error) is always lower than 4%.

In Table 6, some surface properties of the reverse micelle and its water core are reported. We first compare in the columns labeled SRM_v and SRM_e the contact surface between the micelles and the isooctane solvent. The former surfaces were computed by adding up the area of the Voronoi[54] facets shared between the molecules of the micelles and the solvent. Voronoi polyhedrons were constructed according to the algorithm and program provided in ref 55. SRM_e is instead the area of the average micellar ellipsoid derived in section III.A. The comparison of the two values shows unequivocally that the interface between our micelles and the solvent has a large rugosity factor, $f_r = SRM_v/SRM_e$, f_r being between 1.6 and 1.9 for all micelles.

Table 6 also presents the ratio between the solvent accessible surface and the total surface for AOT, ASA_{AOT}, and water, ASA_w. The stable values of ASA_{AOT} for all micelles show that the solvent accessible surface for AOT does not change much with the system size, whereas ASA_w, always close to zero, indicates that for none of the systems studied here does isooctane penetrate inside their hydrophilic region.

The last two columns of Table 6 report the average surface area of AOT in contact with water, a_0. a_0^v was computed by adding up the surface area of each Voronoi polyhedron shared between AOT and water. a_0^e was instead obtained by computing the surface area of an ellipsoid approximating the average shape of the water core and dividing by the number of AOT molecules. Whereas a_0^e remains stable with changes in the system size, a_0^v increases from RM43 to RM82 and reaches a value very close to a_0^e for RM82. Our values of a_0 for RM82 corresponding to $W_0 = 7$ agree well with the estimate of 64 Å^2 obtained from SANS experiments[27] for RMs with $W_0 = 8.16$ and higher. Values for a_0 between 20 and 50 Å^2 are also found in ref 17 for sizes of micelles from $W_0 = 3$ to 30.

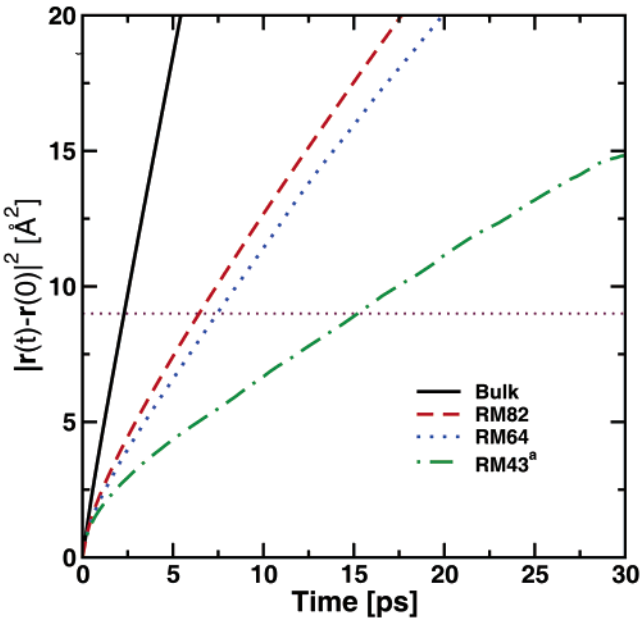

Figure 7. Plot of the mean square displacement of the water oxygen atoms, $\langle|\mathbf{r}(t)|^2\rangle$, versus time, t, for bulk water, RM43^a, RM64, and RM82.

TABLE 7: Diffusion of Water in Reverse Micelles and Bulk^a

systems	α	τ_w	systems	α	τ_w
bulk	0.98	2.4	RM64	0.87	7.5
RM43^a	0.67	15.9	RM82	0.80	6.5

^{a} α is the dispersion regime parameter obtained by nonlinear fitting of the $\langle|\mathbf{r}(t)|^2\rangle$ values of Figure 7. τ_w is a measure of the residence time defined as the time employed by a molecule to cover a distance equivalent to its own diameter; for water, this is 3 Å.

We have also investigated the translational diffusion of water in the hydrophilic core by monitoring the mean square displacement of the water oxygens, or $\langle|\mathbf{r}(t)|^2\rangle$. In Figure 7, we show this function for the micelles RM43^a, RM64, and RM82 and compare with the result for bulk water. The difference between diffusion of water in the bulk and in the reverse micelle core is striking: for all micelles investigated, water is in a dispersive diffusion regime[56] and obeys a law

$$\langle|\mathbf{r}(t)|^2\rangle \propto t^{\alpha}$$

The value of α is smaller for the smallest micelle, α = 0.66, and increases to ≃0.8 for the largest ones; see Table 7. For RM43^a, the value of α is very similar with results (α ≃ 0.6) obtained by some of us for the diffusion of hydration water of proteins.[56] We remark that here all water molecules contribute to the calculation of $\langle|\mathbf{r}(t)|^2\rangle$, whereas in ref 56 we only considered contributions from hydration water. This explains that for the RM43^a, where almost all waters are in contact with AOT, α is smaller. Its value increases with the size of the water core, i.e., with the number of waters outside the first hydration shell.

For a nonlinear diffusion regime such as that of water in our reverse micelles, it is convenient to use the residence time, τ_w, as a measure of the diffusion intensity. As in a previous work,[56] we define τ_w as the time required by a molecule to cover a distance equivalent to its own diameter, which is ≃3 Å for water. Thus, in Figure 7, τ_w is the time for the $\langle|\mathbf{r}(t)|^2\rangle$ values to reach 9 Å^2. The values of τ_w, collected in Table 7, show that in RM43^a water is retarded 6.6 times that of the bulk, which is very close to our findings for hydration water in proteins and also similar to findings on RMs of perfluoropolyether surfactants.[22] Retardation in translational diffusion decreases to 3 for the largest micelles.

D. Summary and Conclusion. Our theoretical investigation is the first to provide a fully atomistic molecular model for reverse micelles of AOT in an apolar solvent. We have addressed the problem of the shape and structure of the micelle as a whole and of the confined water in its interior. We find that all micelles studied here are nonspherical and present an ellipsoidal shape with eccentricity factors $e = 0.60-0.70$. The confined water of the micelle inner core also presents an ellipsoidal shape with larger eccentricity, $e \simeq 0.80$. These results appear robust as two simulations, carried out for $W_0 = 3$ from independent initial conditions, produced two ellipsoidal micelles that were very similar, although not identical, in shape and dimensions.

We point out to the reader that our study did not intend to fully address the problem of the size of the micelles. Microemulsions formed by the AOT−water−oil system are likely polydisperse in nature, whereas our simulations, evidently, involved only monodisperse systems. In our case, the aggregation number drives entirely the dimensions of the reverse micelle. Nevertheless, good agreement is found between the average radius of our micelles and that estimated from Guinier-like analysis of SAXS experiments.[29] Also, the linear dependence of $\bar{R}^w$ versus W_0 remarked in SANS experiments[27,28] is well reproduced by our simulations. Thus, we find a slope and an intercept which are between the experimental SANS estimates. Nevertheless, we notice that our estimates of the water core volume differ with those estimated in ref 17. We remark that a non-negligible surfactant density was found in the inner core of the smallest micelles, thus reducing the density of the water pool. This finding should be taken into account in the interpretation of SAXS studies of small reverse micelles.

Consistently with previous simulations of other RM systems,[19] the interface between oil and the hydrophobic chains of AOT is highly corrugated, with rugosity factors larger than 1.6. Our simulations show that between 31 and 35% of the total AOT surface (565 Å^2 averaged over the four runs) is shared with the oil, while between 52 and 67 Å^2 is in common between AOT and water. The latter values are in good agreement with the estimate of ≃64.1 Å^2 obtained from SANS experiments on reverse micelles of size larger than ours, $W_0 = 8.1-50$.[27] Finally, we find that the water of the inner core is sturdily protected from oil, as less than 1% of the water surface comes in direct contact with isooctane.

We have also investigated the behavior of the confined water in the inner core. From smaller micelles to larger, we find that water tends to draw closer in its properties to those of bulk water. Significant is that the hydration of the sodium ion is eased by the increases of W_0, as shown by the larger number of water neighbors for RM82. The trend toward bulk properties is also observed in the behavior of the mean square displacement of the water oxygen atoms. We estimated that diffusion in the smaller micelle is 6.6 times slower than in the bulk, whereas in larger micelles the retardation is smaller, with the contribution from bulklike diffusing molecules increasing. Our result on the smallest micelle closely matches the results of Berkowitz and co-workers on a reverse micelle in critical CO_2.[57]

To conclude, we point out that our paper is a first and necessary step to improve our atomic level knowledge of AOT−water ionic micelles. In the future, the molecular modeling of the AOT−water−oil system will be used to investigate the

properties of confined water to respond to pressure changes and to solubilize biomolecules, such as peptides and small proteins.

Acknowledgment. Two of the authors (S.A. and M.M.) thank Marcel Waks and Wladimir Urbach for useful discussions and a critical reading of this manuscript. One of us, S.A., is grateful for financial support from AGEFIPH (Association de gestion des fonds pour l'insertion professionnelle des personnes handicappées).

Supporting Information Available: Potential parameters and topology for di-2-ethylhexylsulfoccinate, AOT, and isooctane. This material is available free of charge via the Internet at http://pubs.acs.org.

References and Notes

(1) Hoar, T.; Schulman, J. *Nature* (*London*) **1943**, *152*, 102.
(2) Fendler, J.; Fendler, E. *Catalysis in Micellar and Macromolecular Systems*; Academic Press: New York, 1975.
(3) Martinek, K.; Levashov, A. V.; Khelnitzki, Y. L.; Berezin, J. V. *Dokl. Acad. Nauk. SSSR* **1977**, *236*, 920−923.
(4) Chang, G.; Huang, E.; Hung, H. *Proc. Natl. Sci. Counc.* **2000**, *24*, 89−100.
(5) Fendler, J. *Membrane Mimetic Chemistry*; Wiley: New York, 1982.
(6) Waks, M. *Proteins: Struct. Funct. Genet.* **1986**, *1*, 4−15.
(7) Lang, J.; Jada, A.; Malliaris, A. *J. Chem. Phys.* **1988**, *92*, 1946−1953.
(8) Silber, J.; Biasutti, A.; Abuin, E.; Lissi, E. *Adv. Colloid Interface Sci.* **1999**, *82*, 189.
(9) Maitra, A. *J. Phys. Chem.* **1984**, *88*, 5122−5125.
(10) Hauser, H.; Haering, G.; Pande, A.; Luisi, P. *J. Phys. Chem.* **1989**, *93*, 7869−7876.
(11) Kotlarchyk, M.; Chen, S. *J. Chem. Phys.* **1983**, *79*, 2561−2567.
(12) Boyd, J.; Brisman, A.; Colvin, V.; Mittleman, D. *Phys. Rev. Lett.* **2001**, *87*, 147.
(13) Venables, D.; Huang, K.; Schmuttenmaer, C. *J. Phys. Chem. B* **2001**, *105*, 9132−9138.
(14) Mittleman, D.; Nuss, M.; Colvin, M. *Chem. Phys. Lett.* **1997**, *275*, 332−338.
(15) Eicke, H.; Rehak, J. *Helv. Chim. Acta* **1976**, *59*, 2883−2891.
(16) Chatenay, D.; Urbach, W.; Nicot, C.; Vacher, M.; Waks, M. *J. Phys. Chem.* **1987**, *91*, 2196−2201.
(17) Amararene, A.; Gindre, M.; Huerou, J. L.; Urbach, W.; Valdez, D.; Waks, M. *Phys. Rev. E* **2000**, *61*, 682−689.
(18) Tobias, D. J.; Klein, M. L. *J. Phys. Chem.* **1996**, *100*, 6637−6648.
(19) Allen, R.; Bandyopadhyay, S.; Klein, M. *Langmuir* **2000**, *16*, 10547−10552.
(20) Salaniwal, S.; Cui, S.; Cummings, P.; Cochran, H. *Langmuir* **1999**, *15*, 5188−5192.
(21) Salaniwal, S.; Cui, S.; Cochran, H.; Cummings, P. *Langmuir* **2001**, *17*, 1773−1783.
(22) Senapati, S.; Berkowitz, M. *J. Phys. Chem. B* **2003**, *107*, 12906−12916.
(23) Senapati, S.; Berkowitz, M. *J. Chem. Phys.* **2003**, *118*, 1937−1944.
(24) Day, R.; Robinson, B.; Clarke, J.; Doherty, J. *J. Chem. Soc., Faraday Trans.* **1979**, *75*, 132.
(25) Kotlarchyk, M.; Chen, S. H.; Huang, J. S.; Kim, M. W. *Phys. Rev. A* **1984**, *29*, 2054.
(26) Cabos, C.; Delord, P. *J. Appl. Crystallogr.* **1979**, *12*, 502.
(27) Kotlarchyk, M.; Chen, S.; Huang, J. *J. Phys. Chem.* **1982**, *86*, 3273−3276.
(28) Lipgen, S.; Schuebel, D.; Schlicht, L.; Spilgies, J.-H.; Ilgenfritz, G.; Estoe, J.; Heenan, R. K. *Langmuir* **1998**, *14*, 1041−1049.
(29) Yano, J.; Furedi-Milhofer, H.; Watchel, E.; Garti, N. *Langmuir* **2000**, *16*, 9996.
(30) Levinger, N. *Science* **2002**, *298*, 1722−1723.
(31) Boyd, J. E.; Briskman, A.; Sayes, C. M.; Mittleman, D.; Colvin, V. *J. Phys. Chem. B* **2002**, *106*, 6346−6353.
(32) Brown, D.; Clark, H. *J. Phys. Chem.* **1988**, *92*, 2881−2888.
(33) Linse, P. *J. Chem. Phys.* **1989**, *90*, 4992−5004.
(34) Faeder, J.; Ladanyi, B. *J. Phys. Chem. B* **2000**, *104*, 1033−1046.
(35) Faeder, J.; Ladanyi, B. *J. Phys. Chem. B* **2001**, *105*, 11148−11158.
(36) Pileni, M. *Structure and reactivity in reverse micelles*; Elsevier: Amsterdam, 1989.
(37) Schlenkrich, M.; Brickmann, J.; MacKerell, A. D.; Karplux, M. In *Biological Membranes*: *A Molecular Perspective from Computation and Experiment*; Birkhauser: Boston, 1996.
(38) Chanda, J.; Chakraborty, S.; Bandyopadhyay, S. Submitted.
(39) Jorgensen, W.; Chandrasekhar, J.; Madura, J. *J. Chem. Phys.* **1983**, *79*, 926−935.
(40) Andersen, H. *J. Phys. Chem.* **1980**, *72*, 2384−2393.
(41) Parinello, M.; Rahman, A. *J. Appl. Phys.* **1981**, *52*, 7182−7190.
(42) Nose, S. *J. Phys. Chem.* **1984**, *81*, 511−519.
(43) Hoover, W. *Phys. Rev. A* **1985**, *31*, 1695−1697.
(44) Marchi, M.; Procacci, P. *J. Chem. Phys.* **1998**, *109*, 5194−5202.
(45) Tuckerman, M. E.; Berne, B. J.; Martyna, G. A. *J. Chem. Phys.* **1992**, *97*, 1990−2001.
(46) Essmann, U.; Perera, L.; Berkowitz, M. L.; Darden, T.; Lee, H.; Pedersen, L. G. *J. Chem. Phys.* **1995**, *103*, 8577−8593.
(47) Procacci, P.; Darden, T. A.; Paci, E.; Marchi, M. *J. Comput. Chem.* **1997**, *18*, 1848−1862.
(48) Robinson, B. H.; Toprakcioglu, C.; Dore, J.; Chieux, O. *J. Chem. Soc., Faraday Trans.* **1984**, *80*, 13−27.
(49) Merdas, A.; Gindre, M.; Ober, R.; Nicot, C.; Urbach, W.; Waks, M. *J. Phys. Chem.* **1995**, *99*, 1846−1855.
(50) Senapati, S.; Keiper, J.; DeSimone, J.; Wignall, G.; Melnichenko, Y.; Frielinghaus, H.; Berkowitz, M. *Langmuir* **2002**, *18*, 7371−7376.
(51) Watanabe, K.; Ferrario, M.; Klein, M. *J. Phys. Chem.* **1988**, *92*, 819−821.
(52) Watanabe, K.; Klein, M. *J. Phys. Chem.* **1989**, *93*, 6897−6901.
(53) MacKerell, A. *J. Phys. Chem.* **1995**, *99*, 1846−1855.
(54) Voronoi, G. *J. Reine Angew. Math.* **1908**, *134*, 198−287.
(55) Procacci, P.; Scateni, R. *Int. J. Quantum Chem.* **1992**, *42*, 1515−1528.
(56) Marchi, M.; Sterpone, F.; Ceccarelli, M. *J. Am. Chem. Soc.* **2002**, *124*, 6787−6791.
(57) Bruce, C.; Senapati, S.; Berkowitz, M.; Perera, L.; Forbes, M. *J. Phys. Chem. B* **2002**, *104*, 10902−10907.
(58) For sampling reasons, the density at less than 3 Å from the origin is affected by a statistical error of more than 20%.